CLOSED FORM OPTIMIZED TRANSMISSION CONDITIONS FOR COMPLEX DIFFUSION WITH MANY SUBDOMAINS

V. DOLEAN[*], M. J. GANDER[†], AND A. KYRIAKIS[‡]

Abstract. Optimized transmission conditions in domain decomposition methods have been the focus of intensive research efforts over the past decade. Traditionally, transmission conditions are optimized for two subdomain model configurations, and then used in practice for many subdomains. We optimize here transmission conditions for the first time directly for a sequential decomposition into many subdomains and a class of constant coefficient complex diffusion problems. Our asymptotic analysis leads to closed form optimized transmission conditions for many subdomains, and shows that the asymptotic best choice in the mesh size only differs from the two subdomain best choice in the constants, for which we derive the dependence on the number of subdomains explicitly, including the limiting case of an infinite number of subdomains, leading to new insight into scalability. Our results include both Robin and Ventcell transmission conditions, and we also optimize for the first time a two-sided Ventcell condition. We illustrate our results with numerical experiments, both for situations covered by our analysis and situations that go beyond.

Key words. Optimized transmission conditions, complex diffusion, optimized Schwarz methods, many subdomains.

AMS subject classifications. 65N55, 65N35, 65F10

1. Introduction. Diffusion problems are ubiquitous in science and engineering. While classical diffusion problems are real, there are also important complex diffusion problems. For example in geophysics, the magnetotelluric approximation of Maxwell's equations is a key tool to extract information about the spatial variation of electrical conductivity in the Earth's subsurface [35]. This approximation results in a complex diffusion equation [16] of the form

$$\Delta u - (\eta - i\varepsilon)u = f, \quad \text{in a domain } \Omega, \tag{1.1}$$

where f is the source function, and η and ε are strictly positive constants[1].

We are interested here in designing and analyzing domain decomposition methods for complex diffusion problems of the form (1.1) that use optimized transmission conditions; for an analysis of the performance of the classical Schwarz method for such problems, see [15]. Optimized transmission conditions have their roots in the seminal work of Hagström, Tewarson and Jazcilevich [26], Lions [29], Després [11, 12] and Nataf et. al. [34, 33, 32], with first optimizations in [28, 7, 27]. Traditionally, the transmission conditions are derived and optimized for simple two subdomain configurations, like in optimized Schwarz methods, see [6, 20, 3, 22, 14, 24, 23, 25, 1, 31, 19, 18, 30] and references therein. We investigate here the optimization of transmission conditions directly for the many subdomain case, and also study the optimization problem in the limit when the number of subdomains goes to infinity, using the tool of limiting spectra, see [2] and the references therein. Our analysis for overlapping methods

---

[*]Department of Mathematics and Statistics, University of Strathclyde, Glasgow, UK, and Laboratoire J.A. Dieudonné, CNRS, University Côte d'Azur, Nice, France. E-mail: work@victoritadolean.com.

[†]Section de mathématiques, University of Geneva, Switzerland. E-mail: Martin.Gander@unige.ch

[‡]Department of Mathematics and Statistics, University of Strathclyde, Glasgow, UK, E-mail: Alexandros.Kyriakis@strath.ac.uk.

[1]In the magnetotelluric approximation we have $\eta = 0$, but we consider the slightly more general complex diffusion case here. Note also that the zeroth order term in (1.1) is much more benign than the zeroth order term of opposite sign in the Helmholtz equation, see e.g. [17].

shows that the optimized transmission conditions in the many subdomain case be-have asymptotically when the overlap goes to zero like the optimized transmission conditions for the two subdomain case. The only difference are the constants, which we derive in closed form for a given number of subdomains. We optimize both Robin and Ventcell (second order) transmission conditions, and for the first time also a two-sided variant of the Ventcell conditions. Our results also hold for the classical Laplace problem, by simply setting η and ε to zero. We furthermore get from our analysis a new scalability result for complex diffusion problems, which was first observed in the context of solvation models in [4], and then proved for the Laplace problem in [8], and also holds for other domain decomposition methods in such strip type domain decomposition settings [5], see also [9] for maximum principle techniques and [10] for Lions type projection arguments in more general geometries. We do not consider decompositions with cross-points here, for which new techniques that are just in development now would be needed.

2. Optimized Schwarz methods for many subdomains. Our preliminary results in the short conference proceedings paper [13] have shown that for Robin transmission conditions in the magnetotelluric approximation of Maxwell's equations the asymptotically optimal parameter choice for two and three subdomains has the same dependence on the overlap parameter when it becomes small. We then also explored this dependence with numerical experiments for four, five and six subdomains and the asymptotic dependence remained the same, only the constants seem to depend on the number of subdomains.

We prove here that indeed the asymptotic dependence of the optimized parameters is the same for any number of subdomains, and also derive the precise constants which themselves have a clear dependence on the number of subdomains. Using the technique of limiting spectra, we can even prove this result when the number of subdomains goes to infinity. We therefore have for the first time a formal proof that the classical approach of optimizing transmission conditions for a two subdomain model problem to obtain optimized Schwarz methods is fully justified for their use on many subdomains. We also show this result for Ventcell (second order) transmission conditions, and optimize for the first time a two-sided Ventcell variant.

To study Optimized Schwarz Methods (OSMs) for (1.1), we use a rectangular domain Ω given by the union of rectangular subdomains $\Omega_j := (a_j, b_j) \times (0, \hat{L})$, $j = 1, 2, \ldots, J$, where $a_j = (j-1)L - \frac{\delta}{2}$ and $b_j = jL + \frac{\delta}{2}$, and δ is the overlap, like in [5]. Our OSM computes for iteration index $n = 1, 2, \ldots$

$$
\begin{array}{rcll}
\Delta u_j^n - (\eta - i\varepsilon)u_j^n &=& f & \text{in } \Omega_j, \\
-\partial_x u_j^n + p_j^- u_j^n &=& -\partial_x u_{j-1}^{n-1} + p_j^- u_{j-1}^{n-1} & \text{at } x = a_j, \\
\partial_x u_j^n + p_j^+ u_j^n &=& \partial_x u_{j+1}^{n-1} + p_j^+ u_{j+1}^{n-1} & \text{at } x = b_j,
\end{array}
\tag{2.1}
$$

where p_j^- and p_j^+ are strictly positive parameters in the so called two-sided OSM, see e.g. [21], and we have at the top and bottom homogeneous Dirichlet boundary conditions, and on the left and right homogeneous Robin boundary conditions, i.e we put for simplicity of notation $u_0^{n-1} = u_{J+1}^{n-1} = 0$ in (2.1). The Robin parameters are fixed at the domain boundaries $x = a_1$ and $x = b_J$ to $p_1^- = p_a$ and $p_J^+ = p_b$. By linearity, it suffices to study the homogeneous equations, $f = 0$, and analyze convergence to zero of the OSM (2.1). Expanding the homogeneous iterates in a

Fourier series

$$u_j^n(x,y) = \sum_{m=1}^{\infty} v_j^n(x,\tilde{k})\sin(\tilde{k}y),$$

where $\tilde{k} = \frac{m\pi}{\tilde{L}}$ to satisfy the homogeneous Dirichlet boundary conditions at the top and bottom, we obtain for the Fourier coefficients the equations

$$
\begin{aligned}
\partial_{xx}v_j^n - (\tilde{k}^2 + \eta - i\varepsilon)v_j^n &= 0 & x \in (a_j, b_j), \\
-\partial_x v_j^n + p_j^- v_j^n &= -\partial_x v_{j-1}^{n-1} + p_j^- v_{j-1}^{n-1} & \text{at } x = a_j, \\
\partial_x v_j^n + p_j^+ v_j^n &= \partial_x v_{j+1}^{n-1} + p_j^+ v_{j+1}^{n-1} & \text{at } x = b_j.
\end{aligned}
\tag{2.2}
$$

The general solution of the differential equation is

$$v_j^n(x,\tilde{k}) = c_j e^{-\lambda(\tilde{k})x} + d_j e^{\lambda(\tilde{k})x},$$

where $\lambda = \lambda(\tilde{k}) = \sqrt{\tilde{k}^2 + \eta - i\varepsilon}$. We next define the Robin traces,

$$
\mathcal{R}_-^{n-1}(a_j,\tilde{k}) := -\partial_x v_{j-1}^{n-1}(a_j,\tilde{k}) + p_j^- v_{j-1}^{n-1}(a_j,\tilde{k}),
$$
$$
\mathcal{R}_+^{n-1}(b_j,\tilde{k}) := \partial_x v_{j+1}^{n-1}(b_j,\tilde{k}) + p_j^+ v_{j+1}^{n-1}(b_j,\tilde{k}).
$$

Inserting the solution into the transmission conditions in (2.2), we obtain for the remaining coefficients c_j and d_j the linear system

$$
c_j e^{-\lambda a_j}(p_j^- + \lambda) + d_j e^{\lambda a_j}(p_j^- - \lambda) = \mathcal{R}_-^{n-1}(a_j,\tilde{k}),
$$
$$
c_j e^{-\lambda b_j}(p_j^+ - \lambda) + d_j e^{\lambda b_j}(p_j^+ + \lambda) = \mathcal{R}_+^{n-1}(b_j,\tilde{k}),
$$

whose solution is

$$
c_j = \frac{1}{D_j}(e^{\lambda b_j}(p_j^+ + \lambda)\mathcal{R}_-^{n-1}(a_j,\tilde{k}) - e^{\lambda a_j}(p_j^- - \lambda)\mathcal{R}_+^{n-1}(b_j,\tilde{k})),
$$
$$
d_j = \frac{1}{D_j}(-e^{-\lambda b_j}(p_j^+ - \lambda)\mathcal{R}_-^{n-1}(a_j,\tilde{k}) + e^{-\lambda a_j}(p_j^- + \lambda)\mathcal{R}_+^{n-1}(b_j,\tilde{k})),
$$

where $D_j := (\lambda + p_j^+)(\lambda + p_j^-)e^{\lambda(L+\delta)} - (\lambda - p_j^+)(\lambda - p_j^-)e^{-\lambda(L+\delta)}$. We thus arrive for the Robin traces in the OSM at the iteration formula

$$
\mathcal{R}_-^n(a_j,\tilde{k}) = \alpha_j^- \mathcal{R}_-^{n-1}(a_{j-1},\tilde{k}) + \beta_j^- \mathcal{R}_+^{n-1}(b_{j-1},\tilde{k}), \quad j = 2,\ldots,J,
$$
$$
\mathcal{R}_+^n(b_j,\tilde{k}) = \beta_j^+ \mathcal{R}_-^{n-1}(a_{j+1},\tilde{k}) + \alpha_j^+ \mathcal{R}_+^{n-1}(b_{j+1},\tilde{k}), \quad j = 1,\ldots,J-1,
$$

where

$$
\begin{aligned}
\alpha_j^- &:= \frac{(\lambda+p_{j-1}^+)(\lambda+p_j^-)e^{\lambda\delta} - (\lambda-p_{j-1}^+)(\lambda-p_j^-)e^{-\lambda\delta}}{(\lambda+p_{j-1}^+)(\lambda+p_{j-1}^-)e^{\lambda(L+\delta)} - (\lambda-p_{j-1}^+)(\lambda-p_{j-1}^-)e^{-\lambda(L+\delta)}}, & j = 2,\ldots,J, \\
\alpha_j^+ &:= \frac{(\lambda+p_{j+1}^-)(\lambda+p_j^+)e^{\lambda\delta} - (\lambda-p_{j+1}^-)(\lambda-p_j^+)e^{-\lambda\delta}}{(\lambda+p_{j+1}^-)(\lambda+p_{j+1}^+)e^{\lambda(L+\delta)} - (\lambda-p_{j+1}^-)(\lambda-p_{j+1}^+)e^{-\lambda(L+\delta)}}, & j = 1,\ldots,J-1, \\
\beta_j^- &:= \frac{(\lambda+p_j^-)(\lambda-p_{j-1}^-)e^{-\lambda L} - (\lambda-p_j^-)(\lambda+p_{j-1}^-)e^{\lambda L}}{(\lambda+p_{j-1}^+)(\lambda+p_{j-1}^-)e^{\lambda(L+\delta)} - (\lambda-p_{j-1}^+)(\lambda-p_{j-1}^-)e^{-\lambda(L+\delta)}}, & j = 2,\ldots,J, \\
\beta_j^+ &:= \frac{(\lambda+p_j^+)(\lambda-p_{j+1}^+)e^{-\lambda L} - (\lambda-p_j^+)(\lambda+p_{j+1}^+)e^{\lambda L}}{(\lambda+p_{j+1}^+)(\lambda+p_{j+1}^-)e^{\lambda(L+\delta)} - (\lambda-p_{j+1}^+)(\lambda-p_{j+1}^-)e^{-\lambda(L+\delta)}}, & j = 1,\ldots,J-1.
\end{aligned}
\tag{2.3}
$$

Defining the 2×2 matrices

$$T_j^1 := \begin{bmatrix} \alpha_j^- & \beta_j^- \\ 0 & 0 \end{bmatrix}, j = 2, .., J \quad \text{and} \quad T_j^2 := \begin{bmatrix} 0 & 0 \\ \beta_j^+ & \alpha_j^+ \end{bmatrix}, j = 1, .., J-1,$$

we can write the OSM in substructured form (keeping the first and last rows and columns to make the block structure appear), namely

$$
\underbrace{\begin{bmatrix} 0 \\ \mathcal{R}_+^n(b_1,\tilde{k}) \\ \mathcal{R}_-^n(a_2,\tilde{k}) \\ \mathcal{R}_+^n(b_2,\tilde{k}) \\ \vdots \\ \mathcal{R}_-^n(a_j,\tilde{k}) \\ \mathcal{R}_+^n(b_j,\tilde{k}) \\ \vdots \\ \mathcal{R}_-^n(a_{N-1},\tilde{k}) \\ \mathcal{R}_+^n(b_{N-1},\tilde{k}) \\ \mathcal{R}_-^n(a_N,\tilde{k}) \\ 0 \end{bmatrix}}_{\mathcal{R}^n}
=
\underbrace{\begin{bmatrix} & T_1^2 & & & & \\ T_2^1 & & T_2^2 & & & \\ & \ddots & & \ddots & & \\ & & T_j^1 & & T_j^2 & \\ & & & \ddots & & \ddots \\ & & & & T_{N-1}^1 & & T_{N-1}^2 \\ & & & & & T_N^1 \end{bmatrix}}_{T}
\underbrace{\begin{bmatrix} 0 \\ \mathcal{R}_+^{n-1}(b_1,\tilde{k}) \\ \mathcal{R}_-^{n-1}(a_2,\tilde{k}) \\ \mathcal{R}_+^{n-1}(b_2,\tilde{k}) \\ \vdots \\ \mathcal{R}_-^{n-1}(a_j,\tilde{k}) \\ \mathcal{R}_+^{n-1}(b_j,\tilde{k}) \\ \vdots \\ \mathcal{R}_-^{n-1}(a_{N-1},\tilde{k}) \\ \mathcal{R}_+^{n-1}(b_{N-1},\tilde{k}) \\ \mathcal{R}_-^{n-1}(a_N,\tilde{k}) \\ 0 \end{bmatrix}}_{\mathcal{R}^{n-1}}.
$$

$$(2.4)$$

If the parameters $p_j^\pm$ are constant over all the interfaces, and we eliminate the first and the last rows and columns of T, T becomes a block Toeplitz matrix. The best choice of the parameters minimizes the spectral radius $\rho(T)$ over a numerically relevant range of frequencies $K := [\tilde{k}_{\min}, \tilde{k}_{\max}]$ with $\tilde{k}_{\min} := \frac{\pi}{\hat{L}}$ and $\tilde{k}_{\max} := \frac{M\pi}{\hat{L}}$, $M \sim \frac{1}{h}$, where h is the mesh size, and is thus solution of the min-max problem

$$\min_{p_j^\pm} \max_{\tilde{k} \in K} \rho(T(\tilde{k}, p_j^\pm)).$$

REMARK 2.1. *This formulation is the most generic possible and the convergence factor in all the other particular cases can be derived from here:*
- *Dirichlet boundary conditions at $x = a_1$ and $x = b_J$ when $p_a, p_b \to \infty$.*
- *Dirichlet transmission conditions at the interfaces between subdomains when $p_j^- \to \infty$, $j = 2, ..., J$ and $p_j^+ \to \infty$, $j = 1, ..., J-1$.*
- *The one dimensional case when λ is replaced by $\lambda(0) = \sqrt{\eta - i\varepsilon}$.*

3. Optimized Robin transmission conditions. We first state without proof the results obtained in the short conference proceedings paper [13] in the two subdomain case before presenting our new results for the case of an arbitrary number of subdomains.

THEOREM 3.1 (Two Subdomain Robin Optimization). *Let $s := \sqrt{\tilde{k}_{\min}^2 + \eta - i\varepsilon}$, where the complex square root is taken with the positive real part, and let K be the real constant*

$$K := \Re \frac{s((p_b + s)(p_a + s) - (s - p_b)(s - p_a)e^{-4sL})}{((s - p_a)e^{-2sL} + s + p_a)((s - p_b)e^{-2sL} + s + p_b)}. \tag{3.1}$$
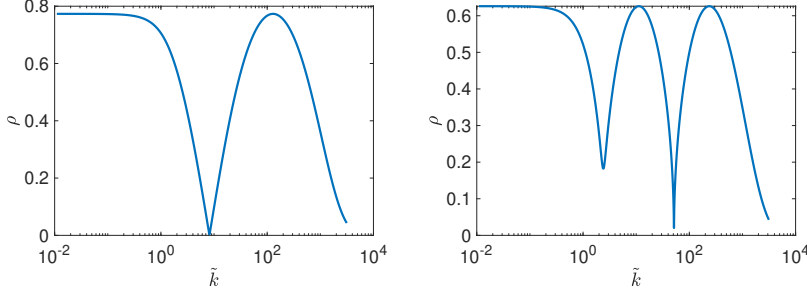
FIG. 3.1. *Equioscillation in numerical optimization with one and two optimized parameters.*

Then for two subdomains with one sided Robin transmission conditions, $p_1^+ = p_2^- =: p$, the asymptotically optimized parameter p for small overlap δ and associated convergence factor are

$$p \sim 2^{-1/3} K^{2/3} \delta^{-1/3}, \quad \rho = 1 - 2^{4/3} K^{1/3} \delta^{1/3} + \mathcal{O}(\delta^{2/3}). \tag{3.2}$$

For two-sided Robin transmission conditions, $p_1^+ \neq p_2^-$, the asymptotically optimized parameters for small overlap δ and associated convergence factor are

$$p_1^+ \sim 2^{-2/5} K^{2/5} \delta^{-3/5}, \; p_2^- \sim 2^{-4/5} K^{4/5} \delta^{-1/5}, \; \rho = 1 - 2^{4/5} K^{1/5} \delta^{1/5} + \mathcal{O}(\delta^{2/5}). \tag{3.3}$$

When Dirichlet BCs are used at $x = a_1$ and $x = b_J$, i.e when p_a and p_b tend to infinity, then the expression of the constant can be further simplified to

$$K := \Re \frac{s(e^{2sL} + 1)}{(e^{2sL} - 1)}.$$

The results of this kind of optimization are illustrated in Figure 3.1 where we see that optimal values are obtained when the convergence factor equioscillates.

3.1. High frequency approximation of T and ρ. It is not possible to directly tackle the optimization of transmission conditions for the many subdomain case, since the spectral radius of the iteration matrix T in (2.4) is a too complex object. There is however an important observation: in the optimization process, we see in Figure 3.1 that the convergence factor, i.e. the spectral radius of T, equioscillates at different frequency points $\tilde{k}$, and the local maximum points are for $\tilde{k}$ large, which motivates the interest of the following Lemma (see also [24, 6] for similar high frequency approximations):

LEMMA 3.2 (High frequency approximation of ρ). *For high frequencies, $\tilde{k}$ large, the convergence factor for $p_j^+ = p_j^- = p$ behaves like*

$$\rho \sim \rho_{1,hf} = \left| \frac{\lambda - p}{\lambda + p} e^{-\lambda \delta} \right|, \tag{3.4}$$

and for p_j^+, $p_{j+1}^- \in \{p_1, p_2\}$ and $p_j^+ \neq p_{j+1}^-$, $j = 1, \dots, J-1$, it behaves like

$$\rho^2 \sim \rho_{2,hf}^2 = \left| \frac{\lambda - p_1}{\lambda + p_1} \cdot \frac{\lambda - p_2}{\lambda + p_2} e^{-2\lambda \delta} \right|. \tag{3.5}$$

Proof. When $\tilde{k}$ is large, the real part of $\lambda(\tilde{k})$ is large as well, and from Equation (2.3) we obtain because of the terms $e^{\lambda L}$ that for $\tilde{k} \to \infty$

$$\alpha_j^{\pm}(\tilde{k}) \sim 0, \quad \beta_j^{-}(\tilde{k}) \sim -\frac{\lambda - p_j^{-}}{\lambda + p_{j-1}^{+}} e^{-\lambda\delta}, \quad \beta_j^{+}(\tilde{k}) \sim -\frac{\lambda - p_j^{+}}{\lambda + p_{j+1}^{-}} e^{-\lambda\delta}.$$

The iteration matrix T thus behaves for $\tilde{k}$ large like

$$T \sim T_{hf} = \begin{bmatrix} 0 & \beta_1^{+} & 0 & 0 & \ldots & 0 & 0 \\ \beta_2^{-} & 0 & 0 & 0 & \ldots & 0 & 0 \\ 0 & 0 & 0 & \beta_2^{+} & \ldots & 0 & 0 \\ 0 & 0 & \beta_3^{-} & 0 & \ldots & 0 & 0 \\ 0 & 0 & \ldots & \ddots & \ddots & 0 & 0 \\ 0 & 0 & \ldots & 0 & 0 & 0 & \beta_{J-1}^{+} \\ 0 & 0 & \ldots & 0 & 0 & \beta_J^{-} & 0 \end{bmatrix}. \tag{3.6}$$

The eigenvalues of this matrix are given by the pairs $\pm\sqrt{\beta_j^{+}\beta_{j+1}^{-}}$, $j = 1, .., J - 1$ and therefore the high frequency convergence factor is

$$\rho_{hf} = \max_j \left| \sqrt{\frac{(\lambda - p_j^{-})(\lambda - p_j^{+})}{(\lambda + p_{j-1}^{+})(\lambda + p_{j+1}^{-})}} e^{-\lambda\delta} \right|,$$

which leads to the result of the lemma. $\square$

This result can also be understood intuitively: the coefficients $\alpha_j^{\pm}$ relate interface values across subdomains, while the coefficients $\beta_j^{\pm}$ relate interface values across the overlap only, which is much smaller than the subdomain size. Since high frequencies are damped rapidly in a diffusion problem over spatial distance, only the terms $\beta_j^{\pm}$ related to the small overlap remain relevant for the high frequency behavior of the algorithm. This is why we see in Equation (3.4) and Equation (3.5) the typical two subdomain convergence factors, see e.g. [18], i.e in optimized Schwarz methods with many subdomains, high frequencies still converge like if there were only two subdomains.

3.2. Optimization for J subdomains. The high frequency behavior of the convergence factor allows us to study systematically the asymptotic form of the best parameter choice for J subdomains, depending on one remaining constant only:

LEMMA 3.3 (Generic optimized Robin asymptotics). *The best choice in the one sided Robin transmission conditions is $p_j^{+} = p_j^{-} = p^*$, and when the overlap δ goes to zero, we have*

$$p^* = \frac{C_k^2}{2}\delta^{-1/3} \quad \Longrightarrow \quad \rho^* \sim 1 - 2C_k\delta^{1/3}, \tag{3.7}$$

where the constant C_k depends on the number of subdomains. In the two-sided Robin transmission condition, the best choice is $p_j^{+}, p_{j+1}^{-} \in \{p_1^*, p_2^*\}$, $p_j^{+} \neq p_{j+1}^{-}$, $j = 1, \ldots, J - 1$, with

$$p_1^* = C_{k_2}^2\delta^{-3/5} \quad p_2^* = C_{k_2}^4\delta^{-1/5} \quad \Longrightarrow \quad \rho^* \sim 1 - 2C_{k_2}\delta^{1/5}. \tag{3.8}$$

Proof. In the one parameter case, we know from [18] that for $\rho_{1,hf}$ from Equation (3.4) the optimal parameter $p^* = C_p \delta^{-1/3}$, and a local maximum of $\rho_{1,hf}$ can be found at[2] $k^* = C_k \delta^{-2/3}$. The relation between the two constants is $C_p = \frac{C_k^2}{2}$, as shown in detail in [13, Proof of Theorem 1], and the maximum of the convergence factor is

$$\rho(k^*) = 1 - 2C_k \delta^{1/3} + \mathcal{O}(\delta^{2/3}), \tag{3.9}$$

which proves the first claim.

For two-sided Robin transmission conditions, the optimal parameters for the high frequency approximation $\rho_{2,hf}$ of the convergence factor from Equation (3.5) were studied in [18], and they verify $p_1^*, p_2^* \in \{C_{k_2}^2 \delta^{-3/5}, C_{k_2}^4 \delta^{-1/5}\}$, with the corresponding maximum of the convergence factor given by

$$\rho(k^*) = 1 - 2C_{k_2} \delta^{1/5} + \mathcal{O}(\delta^{2/5}), \tag{3.10}$$

which proves the second claim. $\square$

It remains to study the constants C_k and C_{k_2}, which are determined by equioscillation with the low frequency convergence factor, i.e. $\rho(\tilde{k}_{min})$, see Figure 3.1, and which depends on the number of subdomains, since we really need to evaluate the spectral radius of the iteration matrix T in (2.4). To simplify the computations, we assume Dirichlet boundary conditions at the outer boundaries of the global domain, that is consider the limits when p_a and p_b go to infinity. We start by computing the leading order terms in T for small overlap δ. For one sided Robin transmission conditions, $p = C_p \delta^{-1/3} = \frac{C_k^2}{2} \delta^{-1/3}$, we obtain, with $s := \sqrt{\tilde{k}_{\min}^2 + \eta - i\varepsilon}$,

$$\alpha_j^+(\tilde{k}_{\min}) = \alpha_j^-(\tilde{k}_{\min}) \sim \frac{4se^{-sL}}{C_p(1 - e^{-2sL})} \delta^{1/3} = \frac{8se^{-sL}}{C_k^2(1 - e^{-2sL})} \delta^{1/3} := \tilde{a},$$

$$\beta_j^+(\tilde{k}_{\min}) = \beta_j^-(\tilde{k}_{\min}) \sim 1 - \frac{2s(e^{-2sL} + 1)}{C_p(1 - e^{-2sL})} \delta^{1/3} = 1 - \frac{4s(e^{-2sL} + 1)}{C_k^2(1 - e^{-2sL})} \delta^{1/3} =: \tilde{b},$$

which leads to the simplified low frequency iteration matrix

$$T_{lf,1par} = \begin{bmatrix}
0 & \tilde{b} & \tilde{a} & 0 & \ldots & 0 & 0 \\
\tilde{b} & 0 & 0 & 0 & \ldots & 0 & 0 \\
0 & 0 & 0 & \tilde{b} & \ldots & 0 & 0 \\
0 & \tilde{a} & \tilde{b} & 0 & \ldots & \tilde{a} & 0 \\
0 & 0 & \ldots & \ddots & \ddots & 0 & 0 \\
0 & 0 & \ldots & 0 & 0 & 0 & \tilde{b} \\
0 & 0 & \ldots & 0 & \tilde{a} & \tilde{b} & 0
\end{bmatrix}. \tag{3.11}$$

By computing the spectral radius of this matrix for $J = 2, 3, 4, \ldots$ subdomains, we

---

[2]It suffices to note that $\lambda = \sqrt{\tilde{k}^2 + \eta - i\varepsilon} \sim |\tilde{k}|$ for $\tilde{k}$ large to see that the results of [18] apply in the high frequency approximation.

get for small overlap δ

$$\rho_2(\tilde{k}_{\min}) \sim 1 - \tfrac{4}{C_k^2} \Re \tfrac{s(e^{2sL}+1)}{(e^{2sL}-1)} \delta^{1/3},$$
$$\rho_3(\tilde{k}_{\min}) \sim 1 - \tfrac{4}{C_k^2} \Re \tfrac{s(e^{2sL}+1-e^{sL})}{(e^{2sL}-1)} \delta^{1/3},$$
$$\rho_4(\tilde{k}_{\min}) \sim 1 - \tfrac{4}{C_k^2} \Re \tfrac{s(e^{2sL}+1-\sqrt{2}e^{sL})}{(e^{2sL}-1)} \delta^{1/3}, \tag{3.12}$$
$$\vdots$$
$$\rho_J(\tilde{k}_{\min}) \sim 1 - \tfrac{4}{C_k^2} \Re \tfrac{s(e^{2sL}+1-2\cos\left(\frac{\pi}{J}\right)e^{sL})}{(e^{2sL}-1)} \delta^{1/3}.$$

Now defining the new constant that appears,

$$K_J := \Re \frac{s(e^{2sL} + 1 - 2\cos\left(\frac{\pi}{J}\right) e^{sL})}{(e^{2sL} - 1)}, \tag{3.13}$$

we obtain $\rho_J(\tilde{k}_{\min}) \sim 1 - \frac{4K_J}{C_k^2}\delta^{1/3}$, and equating this with the high frequency maximum $\rho(k^*) \sim 1 - 2C_k\delta^{1/3}$ from Equation (3.9) leads to

$$C_k = (2K_J)^{1/3}. \tag{3.14}$$

For two-sided Robin transmission conditions, $p_1, p_2 \in \{C_{p_1}\delta^{-1/5}, C_{p_2}\delta^{-3/5}\} = \{C_{k_2}^2\delta^{-1/5}, C_{k_2}^4\delta^{-1/5}\}$, we obtain

$$\alpha_j^+(\tilde{k}_{\min}) = \alpha_j^-(\tilde{k}_{\min}) = \frac{2se^{-sL}}{C_{p_2}(1-e^{-2sL})}\delta^{1/5} = \frac{2se^{-sL}}{C_{k_2}^4(1-e^{-2sL})}\delta^{1/5} := \tilde{a},$$
$$\beta_j^+(\tilde{k}_{\min}), \beta_{j+1}^-(\tilde{k}_{\min}) \in \{\delta^{2/5}C_{k_2}^2\tilde{b}, \tfrac{1}{\delta^{2/5}C_{k_2}^2}\tilde{b}\}, \; \tilde{b} = 1 - \frac{s(e^{-2sL}+1)}{C_{k_2}^4(1-e^{-2sL})}\delta^{1/5},$$

which leads to the low frequency iteration matrix

$$T_{lf,2par} = \begin{bmatrix} 0 & \tilde{b}_+ & \tilde{a} & 0 & \dots & 0 & 0 \\ \tilde{b}_- & 0 & 0 & 0 & \dots & 0 & 0 \\ 0 & 0 & 0 & \tilde{b}_+ & \dots & 0 & 0 \\ 0 & \tilde{a} & \tilde{b}_- & 0 & \dots & \tilde{a} & 0 \\ 0 & 0 & \dots & \ddots & \ddots & 0 & 0 \\ 0 & 0 & \dots & 0 & 0 & 0 & \tilde{b}_+ \\ 0 & 0 & \dots & 0 & \tilde{a} & \tilde{b}_- & 0 \end{bmatrix}, \tag{3.15}$$

where in fact the couple $\tilde{b}_+ \neq \tilde{b}_-$ can vary along the diagonal but always lays in the set $\{\delta^{2/5}C_{k_2}^2\tilde{b}, \frac{1}{\delta^{2/5}C_{k_2}^2}\tilde{b}\}$ which does not change the eigenvalues of the matrix. By computing the spectral radius of this matrix for $J = 2, 3, 4, \dots$ subdomains we get for small overlap δ

$$\rho_J(k_{\min}) \sim 1 - \frac{K_J}{C_{k_2}^4}\delta^{1/5} \tag{3.16}$$

with the same constant K_J from Equation (3.13), and equating with $\rho(k^*) \sim 1 - 2C_{k_2}\delta^{1/5}$ from Equation (3.10), we obtain

$$C_{k_2} = \frac{K_J}{2^{1/5}}. \tag{3.17}$$

We therefore have, using Lemma 3.3, the following result for the J subdomain decomposition:

THEOREM 3.4 (J Subdomain Robin Optimization). *For J subdomains and one sided Robin transmission conditions, $p_j^+ = p_j^-$, the asymptotically optimized parameters for small overlap δ and associated convergence factor are*

$$p_j^+ = p_j^- = p^* \sim \left(\frac{K_J^2}{2}\right)^{1/3} \delta^{-1/3}, \quad \rho \sim 1 - 2^{4/3} K_J^{1/3} \delta^{1/3}, \qquad (3.18)$$

with the constant K_J from Equation (3.13). For two-sided Robin transmission conditions, $p_j^+ \neq p_j^-$, the asymptotically optimized parameters for small overlap δ and associated convergence factor are

$$p_j^+ = p_+^* \sim \left(\frac{K_J}{2^{1/5}}\right)^2 \delta^{-3/5}, \quad p_j^- = p_-^* \sim \left(\frac{K_J}{2^{1/5}}\right)^4 \delta^{-1/5}, \quad \rho \sim 1 - 2^{4/5} K_J \delta^{1/5},$$
(3.19)

and the role of p_+^* and p_-^* can be switched without changing the result.

3.3. Optimization when J goes to infinity. We now use the limiting spectrum approach to study the optimized parameters when the number of subdomains goes to infinity. To do so, we must assume that the outer Robin boundary conditions use the same optimized parameter as at the interfaces, in order to have the Toeplitz structure needed for the limiting spectrum approach. We state here without proof the result obtained in [13].

THEOREM 3.5 (Infinite Number of Subdomains Robin Optimization). *With all Robin parameters equal, $p_j^- = p_j^+ = p$, the convergence factor of the OSM satisfies the bound*

$$\rho = \lim_{J \to +\infty} \rho(T_{2d}^{OS}) \leq \max\left\{ |\alpha - \beta|, |\alpha + \beta| \right\} < 1,$$

where

$$\alpha = \frac{(\lambda + p)^2 e^{\lambda \delta} - (\lambda - p)^2 e^{-\lambda \delta}}{(\lambda + p)^2 e^{\lambda(L+\delta)} - (\lambda - p)^2 e^{-\lambda(L+\delta)}}, \quad \beta = \frac{(\lambda - p)(\lambda + p)(e^{-\lambda L} - e^{\lambda L})}{(\lambda + p)(\lambda + p)e^{\lambda(L+\delta)} - (\lambda - p)(\lambda - p)e^{-\lambda(L+\delta)}}.$$

The asymptotically optimized parameter and associated convergence factor are

$$p^* = 2^{-1/3} K_\infty^{2/3} \delta^{-1/3}, \quad \rho = 1 - 2^{4/3} K_\infty^{1/3} \delta^{1/3} + \mathcal{O}(\delta^{2/3}), \qquad (3.20)$$

with the constant

$$K_\infty := \Re \frac{s(e^{sL} - 1)}{e^{sL} + 1}. \qquad (3.21)$$

If we allow two-sided Robin parameters, $p_j^- = p^-$ and $p_j^+ = p^+$, the OSM convergence factor satisfies the bound

$$\rho = \lim_{J \to +\infty} \rho(T_{2d}^{OS}) \leq \max\left\{ \left|\alpha - \sqrt{\beta_- \beta_+}\right|, \left|\alpha + \sqrt{\beta_- \beta_+}\right| \right\} < 1,$$

where

$$\alpha = \frac{(\lambda + p^+)(\lambda + p^-)e^{\lambda \delta} - (\lambda - p^+)(\lambda - p^-)e^{-\lambda \delta}}{D}, \quad \beta^\pm = \frac{(\lambda^2 - (p^\mp)^2)(e^{-\lambda L} - e^{\lambda L})}{D},$$
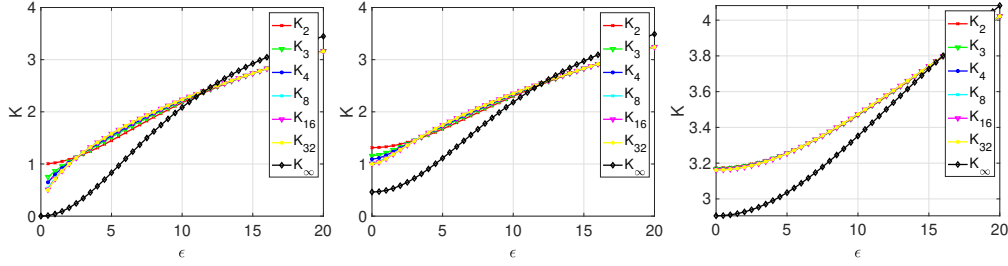
FIG. 3.2. *Optimized constants for different numbers of subdomains for a fixed η and $L = 1$ as a function of ε.*
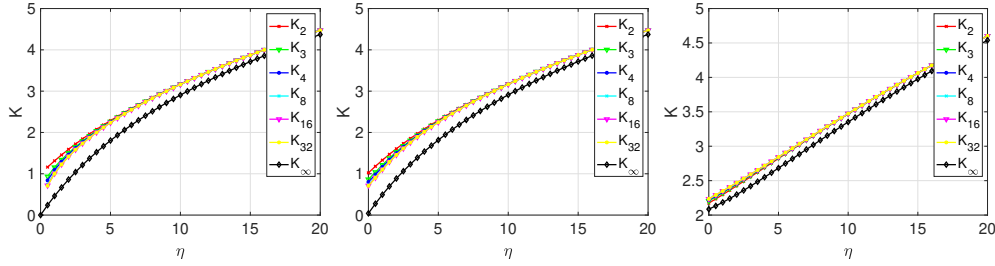

FIG. 3.3. *Optimized constants for different numbers of subdomains for a fixed ε and $L = 1$ as a function of η.*

with $D = (\lambda + p^+)(\lambda + p^-)e^{\lambda(L+\delta)} - (\lambda - p^+)(\lambda - p^-)e^{-\lambda(L+\delta)}$. *The asymptotically optimized parameter choice $p_-^* \neq p_+^*$ and the associated convergence factor are*

$$p_-^*, p_+^* \in \left\{ K_\infty^{2/5}\delta^{-3/5},\ K_\infty^{4/5}\delta^{-1/5} \right\}, \quad \rho = 1 - 2K_\infty^{1/5}\delta^{1/5} + \mathcal{O}(\delta^{2/5}),$$

with the same constant K_∞ as for the one sided case in (3.21).

Even though we had to use Robin outer boundary conditions to obtain K_∞, the constant K_J we obtained for a finite number J of subdomains with Dirichlet boundary conditions converges when J becomes large to K_∞,

$$\lim_{J\to\infty} K_J = \lim_{J\to\infty} \Re \frac{s(e^{2sL} + 1 - 2\cos\left(\frac{\pi}{J}\right)e^{sL})}{(e^{2sL} - 1)} = \Re \frac{s(e^{sL} - 1)}{e^{sL} + 1} = K_\infty. \qquad (3.22)$$

We show in Figures 3.2 and 3.3 how the constants K_J evolve as functions of the problem parameters η and ε for different numbers of subdomains J and how they approach the limiting value K_∞ as the number of subdomains increases. We see that both the two subdomain optimization and the limiting spectrum analysis result for an infinite number of subdomains give quite good approximations for intermediate numbers of subdomains over a large range of problem parameter values, the specific optimization for a given number of subdomains only becomes important when both η and ε are small.

3.4. Scalability. From the constant K_J in (3.13) which governs the convergence factor in Theorem 3.4, and K_∞ in (3.21) which governs the convergence factor when the number of subdomains J goes to infinity in Theorem 3.5, we see that for fixed subdomain width L, K_J is robust when the number of subdomains J increases, and thus our one-level methods are weakly scalable in this setting of strip decompositions,

a result first proved for Laplace problems using different techniques in [8, 9, 10]. Furthermore, we have seen in (3.22) that K_J converges to K_∞ when the number of subdomains J becomes large, which shows that the methods are weakly scalable independently of the outer boundary conditions on the left and right of the strip decomposition. We will illustrate this scalability for fixed L in Subsections 5.2 and 5.3, and also show that scalability is lost when the subdomain size L becomes small when their number J increases, as predicted by the formulas for K_J in (3.13) and K_∞ in (3.21).

4. Optimized Ventcell transmission conditions. To obtain Ventcell (second order) transmission conditions with even better performance, we replace the coefficient $p_j^\pm$ from eq. (2.1) by second order differential operators along the interface. Writing again the local solutions as a Fourier series, the Fourier coefficients satisfy the equations with Ventcell transmission conditions,

$$
\begin{array}{rcll}
\partial_{xx} v_j^n - (\tilde{k}^2 + \eta - i\varepsilon) v_j^n &=& 0 & x \in (a_j, b_j), \\
-\partial_x v_j^n + (p_j^- + \tilde{k}^2 q_j^-) v_j^n &=& -\partial_x v_{j-1}^{n-1} + (p_j^- + \tilde{k}^2 q_j^-) v_{j-1}^{n-1} & \text{at } x = a_j, \\
\partial_x v_j^n + (p_j^+ + \tilde{k}^2 q_j^+) v_j^n &=& \partial_x v_{j+1}^{n-1} + (p_j^+ + \tilde{k}^2 q_j^+) v_{j+1}^{n-1} & \text{at } x = b_j.
\end{array}
\quad (4.1)
$$

As in Section 3, the interface iteration involves a block-Toeplitz iteration matrix which can be obtained by replacing $p_j^\pm$ by $p_j^\pm + \tilde{k}^2 q_j^\pm$ in the matrix from eq. (2.4). The new iteration matrix depends on two sets of parameters, $T_2(\tilde{k}, p_j^\pm, q_j^\pm) := T(\tilde{k}, p_j^\pm + \tilde{k}^2 q_j^\pm)$, and we need to solve now the min-max problem

$$
\min_{p_j^\pm, q_j^\pm} \max_{\tilde{k} \in [\tilde{k}_{min}, \tilde{k}_{max}]} \rho(T_2(\tilde{k}, p_j^\pm, q_j^\pm)).
$$

Like in the case of Robin transmission conditions from Theorem 3.1, we start by showing an optimization result in the case of two subdomains, and then generalize this to the case of many subdomains. We will see that the optimized parameters in the Ventcell case depend on the same constants as for the Robin case.

THEOREM 4.1 (Two Subdomain Ventcell Optimization). *Let* $s := \sqrt{\tilde{k}_{\min}^2 + \eta - i\varepsilon}$, *where the complex square root is taken with the positive real part, and let K be the real constant given in (3.1). Then for two subdomains with one sided Ventcell transmission conditions,* $p_1^+ = p_2^- =: p$, $q_1^+ = q_2^- =: q$, *the asymptotically optimized parameters p and q for small overlap δ and associated convergence factor are*

$$
p \sim 2^{-3/5} K^{4/5} \delta^{-1/5}, \, q \sim 2^{-1/5} K^{-2/5} \delta^{3/5}, \quad \rho \sim 1 - 2^{8/5} K^{1/5} \delta^{1/5} + \mathcal{O}(\delta^{2/5}). \quad (4.2)
$$

For two-sided Ventcell transmission conditions, $p_1^+ \neq p_2^-$, $q_1^+ \neq q_2^-$, *the asymptotically optimized parameters for small overlap δ are*

$$
p_1^+ \sim 2^{-8/9} K^{8/9} \delta^{-1/9}, \, q_1^+ \sim 2^{2/9} K^{-2/9} \delta^{7/9}, \, p_2^- \sim 2^{-2/3} K^{2/3} \delta^{-1/3}, \, q_2^- \sim 2^{4/9} K^{-4/9} \delta^{5/9}
$$
$$
(4.3)
$$

and the associated convergence factor is $\rho \sim 1 - 2^{8/9} K^{1/9} \delta^{1/9} + \mathcal{O}(\delta^{2/9})$.

Proof. The proof follows the lines of the proof of Theorem 3.1 from [13] and uses the fact that the solution of the min-max problem equioscillates, see Figure 4.1. The main difference compared to Robin transmission conditions is that we have now more equioscillations.

In the case of one sided conditions we have two equioscillations $\rho(\tilde{k}_{\min}) = \rho(\tilde{k}_1^*) = \rho(\tilde{k}_2^*)$, where $\tilde{k}_j^*$ are two interior local maxima, and we have asymptotically

$$
p \sim C_p \delta^{-1/5}, q \sim C_q \delta^{3/5}, \rho \sim 1 - C_R \delta^{1/5} + \mathcal{O}(\delta^{2/5}), \tilde{k}_1^* \sim C_{k_1} \delta^{-2/5}, \tilde{k}_2^* \sim C_{k_2} \delta^{-4/5}.
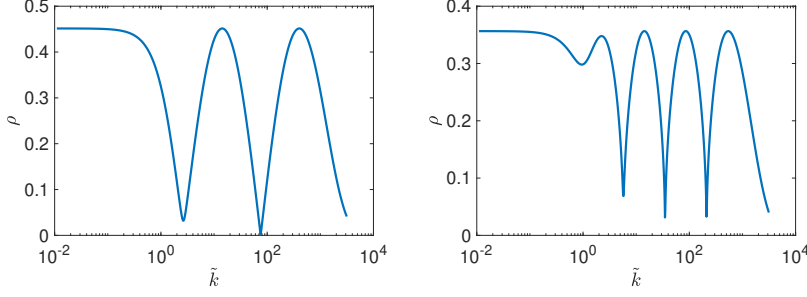$$

FIG. 4.1. *Equioscillation with optimized one sided and two-sided Ventcell transmission conditions.*

By expanding for δ small, and setting the leading terms in the derivatives $\frac{\partial \rho}{\partial k}(\tilde{k}_{1,2}^*)$ to zero, we get $C_p = \frac{2C_{k_1}^2}{C_{k_2}^2}$, $C_q = \frac{2}{C_{k_2}^2}$. Expanding the maxima leads to

$$\rho(\tilde{k}_1^*) \sim 1 - 8\frac{C_{k_1}}{C_{k_2}^2}\delta^{1/5} + \mathcal{O}(\delta^{2/5}), \, \rho(\tilde{k}_2^*) \sim 1 - 2C_{k_2}\delta^{1/5} + \mathcal{O}(\delta^{2/5}),$$

and equating $\rho(\tilde{k}_1^*) = \rho(\tilde{k}_2^*)$ we get $C_{k_1} = \frac{C_{k_2}^3}{4}$ and $C_R = 2C_{k_2}$. Finally equating $\rho(\tilde{k}_{\min}) = \rho(\tilde{k}_2^*)$ asymptotically determines uniquely $C_{k_2} = 2^{3/5}K^{1/5}$ (with K defined in (3.1)) and then $C_{k_1} = 2^{-1/5}K^{3/5}$ and $C_p = 2^{-3/5}K^{4/5}$, $C_q = 2^{-1/5}K^{-2/5}$.

In the case of two-sided conditions, we have four equioscillations, $\rho(k_{\min}) = \rho(\tilde{k}_1^*) = \rho(\tilde{k}_2^*) = \rho(\tilde{k}_3^*) = \rho(\tilde{k}_4^*)$, where $\tilde{k}_j^*$ are four interior local maxima, and we have asymptotically

$$p_1 \sim C_{p_1}\delta^{-1/9}, q_1 \sim C_{q_1}\delta^{7/9}, p_2 \sim C_{p_2}\delta^{-3/9}, q_2 \sim C_{q_2}\delta^{5/9}, \rho \sim 1 - C_R\delta^{1/9} + \mathcal{O}(\delta^{2/9}),$$
$$\tilde{k}_1^* \sim C_{k_1}\delta^{-2/9}, \tilde{k}_2^* \sim C_{k_2}\delta^{-4/9}, \tilde{k}_3^* \sim C_{k_3}\delta^{-6/9}, \tilde{k}_4^* \sim C_{k_4}\delta^{-8/9}.$$

By expanding for δ small, and setting the leading terms in the derivatives $\frac{\partial \rho}{\partial k}(\tilde{k}_{1,2,3,4}^*)$ to zero, we get

$$C_{p_1} = \frac{C_{k_1}^2 \cdot C_{k_3}^2}{C_{k_2}^2 \cdot C_{k_4}^2}, \quad C_{p_2} = \frac{C_{k_2}^2 \cdot C_{k_4}^2}{C_{k_3}^2}, \quad C_{q_1} = \frac{1}{C_{k_4}^2}, \quad C_{q_2} = \frac{C_{k_4}^2}{C_{k_3}^2}. \quad (4.4)$$

Expanding the maxima leads to

$$\rho(\tilde{k}_1^*) \sim 1 - 2\frac{C_{k_1} \cdot C_{k_3}^2}{C_{k_2}^2 \cdot C_{k_4}^2}\delta^{1/9} + \mathcal{O}(\delta^{2/9}), \, \rho(\tilde{k}_2^*) \sim 1 - 2\frac{C_{k_2} \cdot C_{k_4}^2}{C_{k_3}^2 \cdot C_{k_4}^2}\delta^{1/9} + \mathcal{O}(\delta^{2/9}),$$
$$\rho(\tilde{k}_3^*) \sim 1 - 2\frac{C_{k_3}}{C_{k_4}^2}\delta^{1/9} + \mathcal{O}(\delta^{2/9}), \, \rho(\tilde{k}_4^*) \sim 1 - 2C_{k_4}\delta^{1/9} + \mathcal{O}(\delta^{2/9}).$$

Equating now $\rho(\tilde{k}_1^*) = \rho(\tilde{k}_2^*) = \rho(\tilde{k}_3^*) = \rho(\tilde{k}_4^*)$ we get $C_{k_1} = C_{k_4}^7, C_{k_2} = C_{k_4}^5, C_{k_3} = C_{k_4}^3$, $C_R = 2C_{k_4}$ and from (4.4) we get

$$C_{p_1} = C_{k_4}^8, \, C_{p_2} = \frac{1}{C_{k_4}^2}, \, C_{p_3} = C_{k_4}^6, \, C_{p_4} = \frac{1}{C_{k_4}^4}.$$

Finally equating $\rho(\tilde{k}_{\min}) = \rho(\tilde{k}_4^*)$ asymptotically determines uniquely $C_{k_4} = 2^{-1/9}K^{1/9}$ with K given in (3.1) and the other constants are determined accordingly. $\square$

4.1. Optimization for J subdomains. Like in the case of the Robin conditions, the high frequency behavior of the convergence factor allows us to study systematically the asymptotic form of the best parameter choice for J subdomains, depending on one constant only.

LEMMA 4.2 (Generic optimized Ventcell asymptotics). *The best choice for one sided Ventcell transmission conditions is $p_j^+ = p_j^- = p^*$, $q_j^+ = q_j^- = q^*$, and when the overlap δ goes to zero, we have*

$$p \sim \frac{C_{k_2}^4}{8} \delta^{-1/5}, \quad q \sim \frac{2}{C_{k_2}^2} \delta^{3/5}, \qquad \rho \sim 1 - 2C_{k_2}\delta^{1/5} + \mathcal{O}(\delta^{2/5}), \qquad (4.5)$$

where the constant C_{k_2} depends on the number of subdomains. For the two-sided Ventcell transmission conditions, the best choice is $(p_j^+, q_j^+), (p_{j+1}^-, q_{j+1}^-) \in \{(p_1^*, q_1^*), (p_2^*, q_2^*)\}$, $(p_j^+, q_j^+) \neq (p_{j+1}^-, q_{j+1}^-) \, \forall j = 1.., J-1$, with

$$(p_1^*, q_1^*) \sim \left(C_{k_4}^8 \delta^{-1/9}, \frac{1}{C_{k_4}^2} \delta^{7/9} \right), (p_2^*, q_2^*) \sim \left(C_{k_4}^6 \delta^{-3/9}, \frac{1}{C_{k_4}^4} \delta^{5/9} \right), \rho^* \sim 1 - 2C_{k_4}\delta^{1/9},$$
$$(4.6)$$

where the constant C_{k_4} depends again on the number of subdomains.

Proof. Similar to the Robin case in Lemma 3.3, the proof is a direct consequence of Theorem 4.1 where the high frequency arguments are identical in the two or more subdomain case. $\square$

It remains to study the constants C_{k_2} and C_{k_4}, which are determined by equioscillation with the low frequency convergence factor and which depend on the number of subdomains. To simplify the computations, we assume again Dirichlet boundary conditions at the outer boundaries of the global domain and we start by computing the leading order terms in T for small overlap δ. For one sided conditions $p^* = \frac{C_{k_2}^4}{8}\delta^{-1/5}$, $q^* = \frac{2}{C_{k_2}^2}\delta^{3/5}$ we get, with $s := \sqrt{\tilde{k}_{\min}^2 + \eta - i\varepsilon}$,

$$\alpha_j^+(\tilde{k}_{\min}) = \alpha_j^-(\tilde{k}_{\min}) \sim \frac{4se^{-sL}}{C_p(1 - e^{-2sL})}\delta^{1/5} = \frac{32se^{-sL}}{C_k^5(1 - e^{-2sL})}\delta^{1/5} := \tilde{a},$$

$$\beta_j^+(\tilde{k}_{\min}) = \beta_j^-(\tilde{k}_{\min}) \sim 1 - \frac{2s(e^{-2sL} + 1)}{C_p(1 - e^{-2sL})}\delta^{1/5} = 1 - \frac{16s(e^{-2sL} + 1)}{C_k^4(1 - e^{-2sL})}\delta^{1/5} =: \tilde{b},$$

leading to the low frequency iteration matrix of the same form like in Equation (3.11). By computing the spectral radius of this matrix for $J = 2, 3, 4, \ldots$ subdomains, we get for small overlap δ

$$\rho_J(\tilde{k}_{\min}) \sim 1 - \frac{16}{C_{k_2}^4} K_J \delta^{1/3}, \qquad (4.7)$$

with the same constant K_J defined in (3.13), and we obtain $\rho_J(\tilde{k}_{\min}) \sim 1 - \frac{16K_J}{C_{k_2}^4}\delta^{1/5}$. By equating this with the high frequency maximum $\rho(k^*) \sim 1 - 2C_{k_2}\delta^{1/5}$ from (4.5) leads to $C_{k_2} = (8K_J)^{1/5}$.

For the two-sided Ventcell transmission conditions with $(p_1^*, q_1^*) \sim (C_{k_4}^8 \delta^{-1/9}, \frac{1}{C_{k_4}^2}\delta^{7/9})$,

$(p_2^*, q_2^*) = (C_{k_4}^6 \delta^{-3/9}, \frac{1}{C_{k_4}^4} \delta^{5/9})$ we have

$$\alpha_j^+(\tilde{k}_{\min}) = \alpha_j^-(k_{\min}) = \frac{2se^{-sL}}{C_{p_2}(1 - e^{-2sL})} \delta^{1/9} = \frac{2se^{-sL}}{C_{k_4}^4(1 - e^{-2sL})} \delta^{1/9} := \tilde{a},$$

$$\beta_j^+(\tilde{k}_{\min}), \beta_{j+1}^-(k_{\min}) \in \{\delta^{2/9} C_{k_4}^2 \tilde{b}, \frac{1}{\delta^{2/9} C_{k_4}^2} \tilde{b}\}, \quad \tilde{b} := 1 - \frac{s(e^{-2sL} + 1)}{C_{k_4}^8(1 - e^{-2sL})} \delta^{1/9},$$

leading to the low frequency iteration matrix of the same form like in Equation (3.15) where again the couples $\tilde{b}_+ \neq \tilde{b}_-$ can vary along the diagonal but still lay in the set $\{\delta^{2/9} C_{k_4}^2 \tilde{b}, \frac{1}{\delta^{2/9} C_{k_4}^2} \tilde{b}\}$ which does not change the eigenvalues of the matrix. By computing the spectral radius of this matrix for $J = 2, 3, 4, \dots$ subdomains we get for small overlap δ

$$\rho_J(k_{\min}) \sim 1 - \frac{K_J}{C_{k_4}^8} \delta^{1/9} \tag{4.8}$$

with the same constant K_J from Equation (3.13), and equating with $\rho(k^*) \sim 1 - 2C_{k_4}\delta^{1/9}$ from (4.6) we obtain $C_{k_4} = \left(\frac{K_J}{2}\right)^{1/9}$. We therefore get, using Lemma 4.2, the following result for the J subdomain decomposition:

THEOREM 4.3 (*J Subdomain Ventcell Optimization*). *For J subdomains, the best choice in the one sided Ventcell transmission conditions is $p_j^+ = p_j^- = p^*$, $q_j^+ = q_j^- = q^*$, and when the overlap δ goes to zero, we have*

$$p^* \sim 2^{-3/5} K_J^{4/5} \delta^{-1/5}, q^* \sim 2^{-1/5} K_J^{-2/5} \delta^{3/5}, \quad \rho \sim 1 - 2^{8/5} K_J^{1/5} \delta^{1/5} + \mathcal{O}(\delta^{2/5}), \tag{4.9}$$

with the constant K_J from Equation (3.13). For the two-sided Ventcell transmission conditions the best choice is $(p_j^+, q_j^+), (p_{j+1}^-, q_{j+1}^-) \in \{(p_1^*, q_1^*), (p_2^*, q_2^*)\}$, $(p_j^+, q_j^+) \neq (p_{j+1}^-, q_{j+1}^-) \forall j = 1.., J-1$, with

$$(p_1^*, q_1^*) \sim \left(2^{-8/9} K^{8/9} \delta^{-1/9}, 2^{2/9} K^{-2/9} \delta^{7/9}\right), (p_2^*, q_2^*) \sim \left(2^{-2/3} K^{2/3} \delta^{-1/3}, 2^{4/9} K^{-4/9} \delta^{5/9}\right), \tag{4.10}$$

leading to $\rho^* \sim 1 - 2^{8/9} K_J^{1/9} \delta^{1/9}$.

Since the asymptotic convergence factors for Ventcell transmission conditions depend on the same constant K_J as for Robin transmission conditions, the one-level methods with Ventcell transmission conditions have the same scalability properties described in Subsection 3.4 for Robin transmission conditions, and we will illustrate this as well in the following section with numerical experiments.

5. Numerical results. Throughout this section we fix the values of the parameters to $\eta = \varepsilon = 1$. To discretise we use a uniform square grid in each direction and triangulate to form P1 elements. We use an overlap of size $\delta = 4h$, with h being the mesh size. All computations are performed using FreeFem (http://freefem.org/).

5.1. Optimised Schwarz methods as solvers: asymptotic behaviour. We start with a decomposition into four overlapping domains, that can be uniform (four rectangles) or a more general decomposition from METIS as shown in Figure 5.1. We consider one and two-sided Robin and Ventcell transmission conditions, and we increase locally the number of degrees of freedom, which leads to a decreasing value of the mesh size h, and thus the overlap δ. We show results for the iterative version

FIG. 5.1. *Decomposition into four subdomains: uniform (left) and METIS (right).*

h	RAS	Robin 1	Robin 2	Ventcell 1	Ventcell 2
$\frac{1}{50}$	36 (50)	9 (10)	9 (12)	7 (7)	7 (9)
$\frac{1}{100}$	70 (88)	11 (12)	10 (16)	7 (7)	8 (10)
$\frac{1}{200}$	139 (178)	14 (15)	12 (15)	8 (8)	10 (11)
$\frac{1}{400}$	276 (358)	17 (19)	15 (19)	9 (10)	11 (14)
$\frac{1}{800}$	551 (717)	22 (25)	17 (22)	11 (12)	12 (15)
$\frac{1}{1600}$	1100 (1436)	27 (31)	19 (24)	13 (15)	13 (17)

TABLE 5.1
RAS vs. One and two-sided Robin and Ventcell conditions for refined meshes

of the classical Restricted Additive Schwarz method (RAS) and the optimised versions of the algorithm using their ORAS (Optimized Restricted Additive Schwarz) implementation [19]. In Table 5.1 we report the iteration count in order to achieve a relative discrete L^2-norm error reduction of 10^{-6} (the numbers in parentheses correspond to the METIS decompositions). In all tests we start with a random initial guess in order to ensure that all frequencies are present in the error. We see that in the case of the classical Schwarz algorithm (RAS) the iteration count increases linearly when the mesh size representing the overlap is decreased linearly, leading to an important number of iterations for very fine meshes. This statement is true both in the case of uniform and METIS decompositions, and the iteration count for the latter is slightly larger. These results can be greatly improved by using optimised versions of the algorithm, and we notice a progressive improvement of the behaviour, first with Robin and then with Ventcell transmission conditions, as predicted by our analysis.

To see the asymptotic behavior, we plot the iteration counts in Figure 5.2. We see that the results are consistent with the theory, i.e. in the case of Robin 1 (one-sided) transmission conditions, the iteration count increases like $h^{-1/3}$ and in the case of Ventcell 1 like $h^{-1/5}$. For their two-sided variants the iteration count increases like $h^{-1/5}$ for Robin 2 and like $h^{-1/9}$ for Ventcell 2. This behaviour holds both for uniform and METIS decompositions. Note that while the asymptotic behaviour for two-sided Robin and one-sided Ventcell transmission conditions is the same, the iteration count is different, since the constants involved in the theoretical estimates are different. Also, in order to see the full benefit of two-sided Ventcell (Ventcell 2) conditions, highly refined meshes are needed leading to sufficiently large problems: the bottom curves in Figure 5.2 show that two-sided Ventcell conditions will beat the one-sided ones only for more refined meshes than shown here.

5.2. Optimised Schwarz methods as solvers: scalability. We now perform the same kind of experiments but with an increasing number of subdomains and a strip-wise decomposition where we consider again the case of uniform and METIS decompositions. We keep the size of the local subdomains fixed and we choose $h = 1/100$, see Table 5.2. In the case of the classical Schwarz method (RAS), we notice
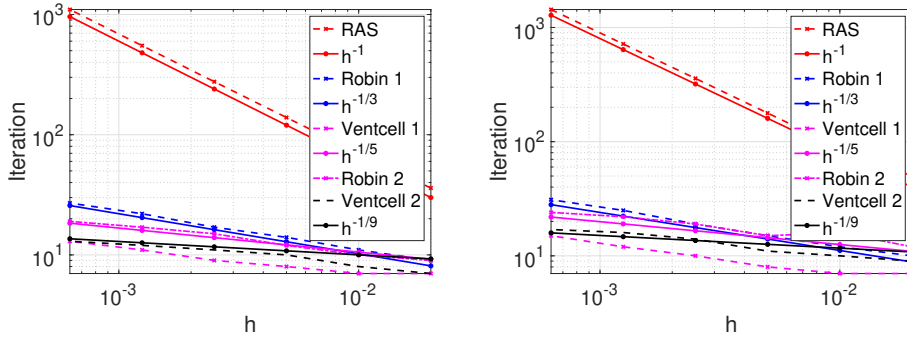
Fig. 5.2. *Iteration count depending on the mesh size for classical Dirichlet (RAS), Robin and Ventcell transmission conditions.*

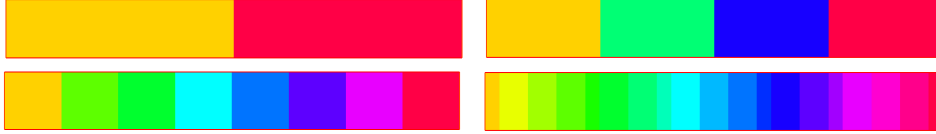| J	RAS	Robin 1	Robin 2	Ventcell 1	Ventcell 2
2	65 (86)	11 (12)	10 (11)	7 (8)	7 (9)
4	70 (88)	11 (12)	10 (11)	7 (8)	7 (9)
8	72 (89)	11 (12)	11 (12)	7 (8)	9 (9)
16	72 (87)	11 (12)	11 (14)	7 (8)	9 (10)
32	73 (89)	11 (12)	11 (15)	7 (8)	9 (10)

TABLE 5.2

RAS vs. one and two-sided Robin and Ventcell conditions for a strip-wise decomposition into J subdomains (fixed subdomain size).

that after a slight increase in iterations when the number of subdomains grows, the iteration count stabilises. This is consistent with the theoretical results and shows that the one-level method is weakly scalable in this setting: the iteration count remains constant when the number of subdomains is increased and the size of the subdomains is kept fixed. The optimised one-level variants are scalable as well, as shown in Subsection 3.4, the iteration counts are much lower, and remain constant almost from the very beginning when the number of subdomains increases. Note that we cannot control the exact size of the subdomains in the case of METIS decompositions, which explains the slight variations in the iteration counts for METIS decompositions. Also the mesh size here is not fine enough to see the full benefit of two sided transmission conditions, see also the comment at the end of the previous subsection.

To see that using the new optimized parameters for many subdomains perform indeed better than the optimized parameters for two subdomains, we run as example the case of 16 subdomains with $\eta = \varepsilon = 0.1$ and meshsize $\frac{1}{800}$ both with the two subdomain optimized parameters (24 iterations) and the new ones for 16 subdomains (22 iterations), which shows that the new parameters indeed perform better, but also that the much simpler two subdomain optimization is already a very viable option.

In a second series of tests, we keep now the size of the global domain fixed to $[0, 8] \times [0, 1]$, and chose the mesh size equal to $h = 1/256$. We increase the number of subdomains in one direction in order to obtain a strip-wise decomposition. In this case, the domains will become thinner and thinner as shown in Figure 5.3.

We see in Table 5.3 that these one level methods are no longer scalable, as predicted by the analysis in Subsection 3.4. The iteration count for RAS grows rapidly with the number of domains. The iteration numbers for Robin 1 and Ventcell 1 are

FIG. 5.3. *Decomposition into many subdomains of decreasing width.*

J	RAS	Robin 1	Robin 2	Ventcell 1	Ventcell 2
2	156	14	12	8	9
4	164	14	13	8	9
8	181	15	13	9	10
16	253	20	17	13	15
32	443	35	54	22	35

TABLE 5.3
RAS vs. one and two-sided Robin and Ventcell conditions for a strip-wise decomposition into J subdomains with decreasing subdomain size.

much lower, but also increase more and more when the number of subdomains doubles, as predicted by the theoretical constants K_J in (3.13) and K_∞ in (3.21) when the subdomain size L becomes small. Furthermore, when two-sided conditions are used, this increase appears to be more important for large J, which is due to the late asymptotic validity of the optimized parameter formulas in this case.

5.3. Optimised Schwarz methods as preconditioners. We solve the discretised problem using GMRES where the parallel Schwarz method with Robin or Ventcell conditions is used as a preconditioner. In particular, we use right-preconditioned GMRES and terminate when a relative residual tolerance of 10^{-6} is reached. The preconditioner, which arises naturally as the discretised version of the parallel Schwarz method we have studied, is known as the one-level optimised restricted additive Schwarz (ORAS) preconditioner. This ORAS preconditioner is given by

$$\mathbf{M}^{-1} = \sum_{i=1}^{N} \mathbf{R}_i^T \mathbf{D}_i \tilde{\mathbf{A}}_i^{-1} \mathbf{R}_i,$$

where $\{\mathbf{R}_i\}_{1 \le i \le N}$ are the Boolean restriction matrices from the global to the local finite element spaces and $\{\mathbf{D}_i\}_{1 \le i \le N}$ are local diagonal matrices representing a partition of unity. The key ingredient of the ORAS method is that the local subdomain matrices $\{\tilde{\mathbf{A}}_i\}_{1 \le i \le N}$ incorporate more efficient Robin or Ventcell transmission conditions.

We now perform exactly the same kind of experiments as in the previous subsections, but test the performance of the preconditioner instead of the stationary iterative solver. We start by the strip-wise decomposition into four subdomains like in Figure 5.1, and we refine the mesh locally in each subdomain. In Table 5.4 we report the iteration count of preconditioned GMRES in order to achieve a relative discrete L^2-norm error reduction of 10^{-6} (the numbers in parentheses correspond to METIS decompositions). Again we start with a random initial guess in order to ensure that all frequencies are present in the error. We see that the iteration count is less sensitive to the choice of transmission conditions, but the hierarchy of the methods is preserved, and iteration counts depend for the optimized methods only very

h	RAS	Robin 1	Robin 2	Ventcell 1	Ventcell 2
$\frac{1}{50}$	12 (17)	6 (7)	7(9)	5 (5)	6 (7)
$\frac{1}{100}$	19 (23)	7 (8)	8 (11)	5 (6)	7 (8)
$\frac{1}{200}$	25 (34)	9 (10)	10 (12)	7 (7)	7 (8)
$\frac{1}{400}$	33 (47)	10 (11)	11 (14)	7 (7)	8 (9)
$\frac{1}{800}$	46 (69)	12 (13)	13 (15)	8 (9)	8 (10)
$\frac{1}{1600}$	69 (93)	14 (15)	14 (15)	9 (10)	8 (10)

TABLE 5.4

GMRES preconditioned by RAS and ORAS with Robin and Ventcell conditions for refined meshes.

J	. RAS	Robin 1	Robin 2	Ventcell 1	Ventcell 2
2	13 (16)	7 (8)	7 (9)	5 (6)	6 (7)
4	19 (23)	7 (8)	8 (11)	5 (6)	7 (8)
8	20 (26)	8 (8)	8 (9)	6 (6)	6 (7)
16	20 (24)	8 (8)	8 (12)	6 (6)	6 (9)
32	20 (26)	8 (8)	8 (12)	6 (6)	6 (9)

TABLE 5.5

GMRES preconditioned by RAS and ORAS with Robin and Ventcell conditions for a strip-wise decomposition into J subdomains (fixed subdomain size).

weakly on the mesh size that represents the overlap. We repeat next the weak scaling experiments from Tables 5.2 and 5.3, where the methods are used as preconditioners. We see in Table 5.5 that also the preconditioners scale very well with the increase of the number of subdomains when the size of the subdomains is kept fixed. However, when the size of the global domain is fixed and the subdomain size decreases when their number increases, we see in Table 5.6 (which corresponds to Table 5.3 but with Schwarz as a preconditioner) that while all methods are convergent, there is a slight but steady increase in the iteration count for all methods, they are not scalable any more, as predicted by the theory.

5.4. General decomposition into subdomains. We next test our new optimized Schwarz methods also in a setting for which we do not yet have a convergence analysis, namely two dimensional uniform and METIS decompositions into 4 subdomains including cross points, like in Figure 5.4.

We show the iteration counts needed by the various preconditioned GMRES methods in Table 5.7. We see that again the optimized variants perform much better than classical RAS, and also the asymptotic dependence on the mesh size representing the overlap is much weaker, so that for larger and larger problems the gain in lower iteration counts is becoming more and more substantial. For example for mesh size $h = \frac{1}{800}$, Robin transmission conditions reduce the iteration count by more than a factor two compared to RAS, and Ventcell transmission conditions by a factor three, at the same cost per iteration.

6. Conclusions. We have shown for the first time that it is possible to optimize transmission conditions for many subdomain decompositions in optimized Schwarz methods. To do so, an essential ingredient was an asymptotic approximation of the convergence factor, and our analysis allowed us to precisely characterize the convergence dependence on the number of subdomains. Using a new technique of limiting spectra, we could even study the case of an infinite number of subdomains, leading

J	RAS	Robin 1	Robin 2	Ventcell 1	Ventcell 2
2	21	9	10	6	7
4	27	9	10	6	6
8	31	9	10	7	8
16	40	13	18	10	10
32	56	20	22	20	18

TABLE 5.6

GMRES preconditioned by RAS vs. one and two-sided Robin and Ventcell conditions for a strip-wise decomposition into J subdomains with decreasing subdomain size.
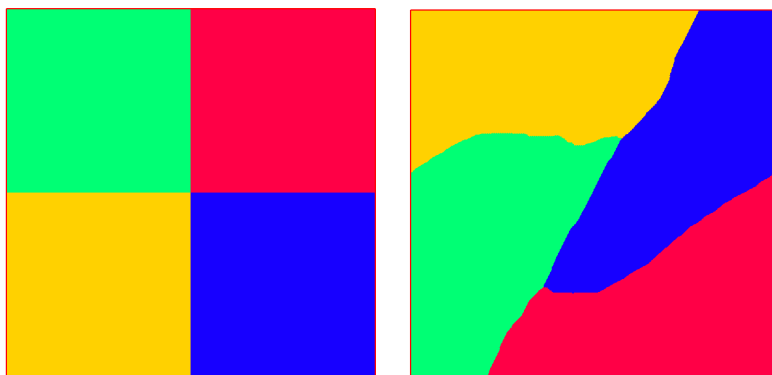

FIG. 5.4. *Decomposition into 4 subdomains (uniform and METIS).*

to a new proof of scalability of these methods for specific strip decompositions for general complex diffusion problems. We also optimized for the first time two-sided Ventcell transmission conditions, which led to a new and much weaker asymptotic dependence on the overlap size than all earlier known optimized Schwarz methods. We illustrated our theoretical results with numerical experiments, including cases not covered by our analysis.

REFERENCES

[1] D. Bennequin, M. J. Gander, L. Gouarin, and L. Halpern. Optimized Schwarz waveform relaxation for advection reaction diffusion equations in two dimensions. *Numerische Mathematik*, 134(3):513–567, 2016.

[2] N. Bootland, V. Dolean, A. Kyriakis, and J. Pestana. Analysis of parallel Schwarz algorithms for time-harmonic problems using block Toeplitz matrices. *Electron. Trans. Numer. Anal.*, 55:112–141, 2022.

[3] R. Brunet, V. Dolean, and M. J. Gander. Natural domain decomposition algorithms for the solution of time-harmonic elastic waves. *SIAM Journal on Scientific Computing*, 42(5):A3313–A3339, 2020.

[4] E. Cancès, Y. Maday, and B. Stamm. Domain decomposition for implicit solvation models. *The Journal of Chemical Physics*, 139:054111, 2013.

[5] F. Chaouqui, G. Ciaramella, and M. Gander. On the scalability of classical one-level domain-decomposition methods. *Vietnam J. Math.*, 46:1053–1088, 2018.

[6] X. Chen, M. J. Gander, and Y. Xu. Optimized Schwarz methods with elliptical domain decompositions. *Journal of Scientific Computing*, 86(2):1–28, 2021.

[7] P. Chevalier and F. Nataf. Symmetrized method with optimized second-order conditions for the Helmholtz equation. In *Domain decomposition methods, 10 (Boulder, CO, 1997)*, pages 400–407. Amer. Math. Soc., Providence, RI, 1998.

h	RAS	Robin 1	Robin 2	Ventcell 1	Ventcell 2
$\frac{1}{50}$	12 (14)	12 (13)	14 (12)	10 (12)	12 (13)
$\frac{1}{100}$	18 (24)	16 (12)	18 (20)	12 (12)	13 (15)
$\frac{1}{200}$	27 (36)	18 (17)	20 (22)	14 (15)	16 (17)
$\frac{1}{400}$	40 (58)	22 (21)	26 (27)	16 (15)	18 (19)
$\frac{1}{800}$	58 (83)	26 (27)	32 (33)	18 (18)	20 (21)

TABLE 5.7

RAS vs. one and two-sided Robin and Ventcell conditions used as preconditioners for GMRES for refined meshes.

[8] G. Ciaramella and M. J. Gander. Analysis of the parallel schwarz method for growing chains of fixed-sized subdomains: Part I. *SIAM Journal on Numerical Analysis*, 55(3):1330–1356, 2017.

[9] G. Ciaramella and M. J. Gander. Analysis of the parallel Schwarz method for growing chains of fixed-sized subdomains: Part II. *SIAM Journal on Numerical Analysis*, 56(3):1498–1524, 2018.

[10] G. Ciaramella and M. J. Gander. Analysis of the parallel Schwarz method for growing chains of fixed-sized subdomains: Part III. *ETNA*, 49:201–243, 2018.

[11] B. Després. Décomposition de domaine et problème de Helmholtz. *C.R. Acad. Sci. Paris*, 1(6):313–316, 1990.

[12] B. Després. Domain decomposition method and the helmholtz problem. *Mathematical and Numerical aspects of wave propagation phenomena*, pages 44–52, 1991.

[13] V. Dolean, M. J. Gander, and A. Kyriakis. Optimizing transmission conditions for multiple subdomains in the Magnetotelluric approximation of Maxwell's equations, 2021.

[14] V. Dolean, M. J. Gander, and E. Veneros. Asymptotic analysis of optimized Schwarz methods for Maxwell's equations with discontinuous coefficients. *ESAIM: Mathematical Modelling and Numerical Analysis*, 52(6):2457–2477, 2018.

[15] F. Donzelli, M. J. Gander, and R. D. Haynes. A schwarz method for the magnetotelluric approximation of Maxwell's equations. In *International Conference on Domain Decomposition Methods*, pages 417–424. Springer, 2018.

[16] F. Donzelli, M. J. Gander, and R. D. Haynes. A Schwarz method for the magnetotelluric approximation of Maxwell's equations, 2019.

[17] O. G. Ernst and M. J. Gander. Why it is difficult to solve Helmholtz problems with classical iterative methods. In *Numerical analysis of multiscale problems*, volume 83 of *Lect. Notes Comput. Sci. Eng.*, pages 325–363. Springer, Heidelberg, 2012.

[18] M. J. Gander. Optimized Schwarz methods. *SIAM Journal on Numerical Analysis*, 44(2):699–731, 2006.

[19] M. J. Gander. Schwarz methods over the course of time. *Electron. Trans. Numer. Anal*, 31(5):228–255, 2008.

[20] M. J. Gander, L. Halpern, F. Hubert, and S. Krell. Optimized Schwarz methods with general Ventcell transmission conditions for fully anisotropic diffusion with discrete duality finite volume discretizations. *Moroccan Journal of Pure and Applied Analysis*, 7:182–213, 2020.

[21] M. J. Gander, L. Halpern, and F. Magoules. An optimized Schwarz method with two-sided Robin transmission conditions for the Helmholtz equation. *International journal for numerical methods in fluids*, 55(2):163–175, 2007.

[22] M. J. Gander and T. Vanzan. Heterogeneous optimized Schwarz methods for second order elliptic PDEs. *SIAM Journal on Scientific Computing*, 41(4):A2329–A2354, 2019.

[23] M. J. Gander and Y. Xu. Optimized Schwarz methods for model problems with continuously variable coefficients. *SIAM Journal on Scientific Computing*, 38(5):A2964–A2986, 2016.

[24] M. J. Gander and Y. Xu. Optimized Schwarz methods with nonoverlapping circular domain decomposition. *Mathematics of Computation*, 86(304):637–660, 2017.

[25] M. J. Gander and H. Zhang. Optimized Schwarz methods with overlap for the Helmholtz equation. *SIAM Journal on Scientific Computing*, 38(5):A3195–A3219, 2016.

[26] T. Hagstrom, R. P. Tewarson, and A. Jazcilevich. Numerical experiments on a domain decomposition algorithm for nonlinear elliptic boundary value problems. *Appl. Math. Lett.*, 1(3), 1988.

[27] C. Japhet, F. Nataf, and F. Rogier. The optimized order 2 method. application to convection-diffusion problems. *Future Generation Computer Systems FUTURE*, 18(1):17–30, 2001.

[28] C. Japhet, F. Nataf, and F.-X. Roux. The Optimized Order 2 Method with a coarse grid preconditioner. application to convection-diffusion problems. In P. Bjorstad, M. Espedal, and D. Keyes, editors, *Ninth International Conference on Domain Decompositon Methods in Science and Engineering*, pages 382–389. John Wiley & Sons, 1998.

[29] P.-L. Lions. On the Schwarz alternating method. III: a variant for nonoverlapping subdomains. In *Third international symposium on domain decomposition methods for partial differential equations*, volume 6, pages 202–223. SIAM Philadelphia, 1990.

[30] V. Martin. An optimized Schwarz waveform relaxation method for the unsteady convection diffusion equation in two dimensions. *Applied Numerical Mathematics*, 52(4):401–428, 2005.

[31] V. Martin. Schwarz waveform relaxation algorithms for the linear viscous equatorial shallow water equations. *SIAM Journal on Scientific Computing*, 31(5):3595–3625, 2009.

[32] F. Nataf. Absorbing boundary conditions in block Gauss-Seidel methods for convection problems. *Math. Models Methods Appl. Sci.*, 6(4):481–502, 1996.

[33] F. Nataf and F. Rogier. Factorization of the convection-diffusion operator and the Schwarz algorithm. M^3AS, 5(1):67–93, 1995.

[34] F. Nataf, F. Rogier, and E. de Sturler. Domain decomposition methods for fluid dynamics, Navier-Stokes equations and related nonlinear analysis. *Edited by A. Sequeira, Plenum Press Corporation*, pages 367–376, 1995.

[35] K. Vozoff. The magnetotelluric method. In *Electromagnetic methods in applied geophysics: Volume 2, application, parts A and B*, pages 641–712. Society of exploration geophysicists, 1991.